RESEARCH ARTICLE

Journal
American Ceramic Society

Two-step reactive flash sintering of high entropy pyrochlore: Densification, grain growth, and microstructural homogeneity

Chen Xu[1] | Jinmao He[1] | Zixu Chen[1] | Guoliang Zhao[1] | Shikui Cai[1] |
Na Ni[2] | Tianwei Liu[1]

[1]Institute of Materials, China Academy of Engineering Physics, Mianyang, China

[2]School of Mechanical Engineering, Shanghai Jiao Tong University, Shanghai, China

Correspondence
Chen Xu, Institute of Materials, China Academy of Engineering Physics, Mianyang, Sichuan, China.
Email: chenxuacademic@163.com

Abstract

Two-step reactive flash sintering (TSRFS) was employed to achieve fast densification of high entropy pyrochlore $(La_{0.2}Nd_{0.2}Sm_{0.2}Eu_{0.2}Gd_{0.2})_2Zr_2O_7$ with suppressed grain growth and improved microstructural homogeneity. Theoretical density of ~98.15% with a grain size of ~684 nm was achieved by TSRFS, representing only half the grain size compared with conventional one-step reactive flash sintering (RFS), while the total holding time of TSRFS was only 1.5 times that of RFS. Although longer duration in step 1 benefited faster densification, it was demonstrated that the shorter time in step 1 not only resulted in smaller grain size in TSRFS samples with identical densities but also helps mitigate the grain size heterogeneity between sample cores and surfaces. Therefore, the art of efficiently using TSRFS lies in the reasonable manipulation of the time and power in step 1 and 2, achieving a balance between densification, grain growth, and microstructural homogeneity.

KEYWORDS
densification, flash sintering, high entropy pyrochlore, microstructural homogeneity, two-step sintering

1 | INTRODUCTION

High-level radioactive waste (HLW) could cause long-term harm to the environment and human health, but the safe disposal of HLW remains a challenge to the sustainable development of the modern nuclear industry.[1] In the past decades ceramic immobilization has been proposed as a promising method for immobilizing HLW, and $A_2B_2O_7$ structured pyrochlore ceramics as an immobilizing matrix has been intensively investigated due to its excellent aqueous durability and irradiation resistance.[2–4] Recent studies suggest that high-entropy pyrochlores exhibit much better aqueous durability and superior irradiation resistance than most pyrochlores including $Gd_2Zr_2O_7$ and $Nd_2Zr_2O_7$.[5,6]

However, the sluggish diffusion effects of high entropy ceramics made the densification rather difficult. For example, although a high temperature heat treatment with long time sintering (e.g., 1500°C for 40 h) may fully densify high entropy pyrochlore,[7] such high temperature treatment probably would cause nuclear elements evaporation and exaggerated grain growth.

Flash sintering (FS) has been developed since 2011, enabling fast densification in minutes at lower furnace temperatures, and hence it has been used to sinter ionic oxides, covalently bonded ceramics, composites, and so on.[8–10] In our previous work, high-entropy pyrochlore $(La_{0.2}Nd_{0.2}Sm_{0.2}Eu_{0.2}Gd_{0.2})_2Zr_2O_7$ was synthesized and consolidated simultaneously within 1 min by flash

sintering at temperatures around 1050°C.[11] Although the raw materials were all nano-sized, the final grain size was still ~1.24 μm due to the rapid final-stage grain growth during flash sintering, which is in a similar fashion to conventional sintering, albeit in a much shorter time scale. Nie et al demonstrated that two-step flash sintering (TSFS) might be a potential method to prepare ceramics with suppressed grain growth.[12] However, samples that undergo flash sintering often exhibit a recurring problem of microstructural heterogeneity, especially in samples with a high surface-to-volume ratio such as dog-bone samples and cylindrical samples.[13] The low thermal conductivity of high-entropy pyrochlore probably would make this problem even worse. Lavagnini et al[13] emphasized that samples sintered by TSFS with high current limit either in step 1 or 2 of TSFS tend to exhibit microstructural heterogeneity. Both current limits and time during flash sintering directly influence the temperature distribution within the specimens and microstructural evolution; hence both of them should be considered comprehensively to investigate the impact of flash sintering on microstructures. However, Lavagnini et al's work[13] dismissed the effects of time.

Herein, a two-step reactive flash sintering (TSRFS) was employed to sintering high-entropy pyrochlore $(La_{0.2}Nd_{0.2}Sm_{0.2}Eu_{0.2}Gd_{0.2})_2Zr_2O_7$, and the effects of the flash sintering curve including time during step 1 and 2 of TSRFS on the microstructural characteristics of $(La_{0.2}Nd_{0.2}Sm_{0.2}Eu_{0.2}Gd_{0.2})_2Zr_2O_7$ were systematically investigated.

2 | EXPERIMENTAL METHODS

Raw materials La_2O_3, Nd_2O_3, Sm_2O_3, Eu_2O_3, Gd_2O_3 and ZrO were mixed according to the stoichiometric mole ratio of $(La_{0.2}Nd_{0.2}Sm_{0.2}Eu_{0.2}Gd_{0.2})_2Zr_2O_7$ in ethanol to form slurries, and the slurries were ball milled in zirconia bottles using zirconia balls for 24 h. Subsequently, the slurries were dried under vacuum at a temperature of 60°C. The dried powders were then ground carefully using an agate mortar. The resultant powders were dry-pressed into dog bone-shaped compacts, measuring 2 cm in length and having a cross-section of 1.1×3 mm, through uniaxial pressing at 3 MPa and followed by cold isostatic pressing at 300 MPa. The green compacts were calcined at 800°C for 2 h in a muffle furnace and then flash sintered.[11] A constant electric field of 150 V/cm was applied to specimens at the start of flash sintering with a heating rate of 5°C/min, and the onsets of flash sintering happened at around 1050°C. For conventional (one-step) flash sintering, the current limit was kept at 0.4 A for different duration as 5 s, 15 s and 30 s (noted as RFS-0.4A-5s, 15s, 30s, respectively). For two-step flash sintering, the current limit was kept at 0.4 A (step 1)

for different duration as 5, 15, and 30 s followed by a current limit at 0.32 A (step 2) for the rest of the time. For example, TSRFS-5–85 s means samples flash sintered in step 1 for 5 s and then in step 2 for 85 s. After flash sintering, both the electric power and the furnace were shut down and samples were cooled down in the furnace. Samples with the same powder processing procedures were pressurelessly sintered at 1600°C for 6 h for comparison and noted as CS-1600°C-6 h. After the flash sintering, samples were cut in their longitudinal middle point and then polished. Figure S1 visually depicts the regions where the micrographs were obtained from the polished surfaces.

The densities of samples were calculated via measuring dimensions and weights, and the Archimedes method was also used if the relative densities were larger than 90%. Relative densities were calculated according to the measured densities and theoretical densities. The crystal structures were characterized by X-ray diffraction (XRD, Rigaku D/max-2400, Tokyo, Japan) using Cu K_α radiation. Raman spectrometer (Renishaw Invia model, Hoffffman Estates, IL) with a 514.5 nm laser was employed to record the Raman spectra. The microstructures were characterized by scanning electron microscopy (SEM, KYKY-EM800, China) with Energy Dispersive X-Ray Spectroscopy (EDS) attached to the SEM.

3 | RESULTS AND DISCUSSION

Figure 1 shows the power, voltage and current curves during TSRFS, in which an increase in electric current is accompanied with a decrease in the value of the applied electric field, and the power shows a spike (stage II) and then rapidly decreases to a relatively low value (stage III). Although the furnace temperature when flash-event occurred in this work was only 1050°C, the real temperature of samples could be much higher than the furnace temperature due to Joule heating,[14,15] which can be estimated by black body radiation (BBR) model.[14] The blackbody radiation equation calculations suggested that the real temperature of the sample at the peak of the power spike was around 1895°C, while the estimated sample temperature corresponding to the current limit of 0.4 and 0.32 A was around 1595 and 1470°C, respectively. The BBR equation used here is as following[11]:

$$\sigma T_0{}^4 + \frac{W}{A\varepsilon} = \sigma T^4, \qquad (1)$$

where T is the real temperature of the sample, and T_0 is the furnace temperature. W is the power dissipation, and A is the surface area of the sample. ε is the emissivity of the specimen, which varies within the range between 0.8 and
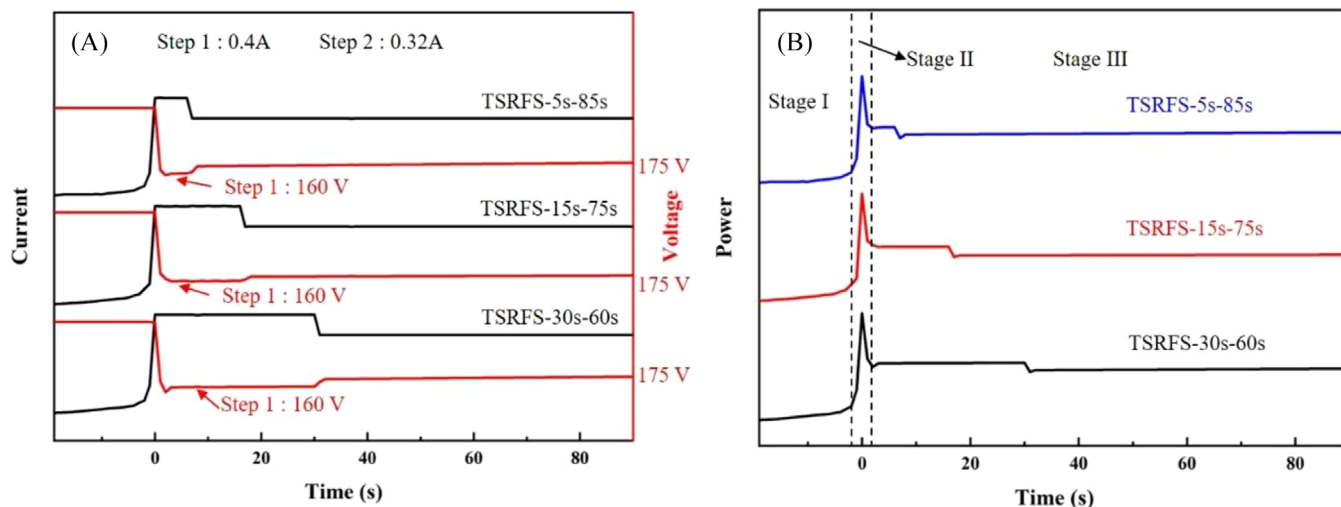
FIGURE 1 Plots of power, voltage, and current during two-step reactive flash sintering (TSRFS) processes.
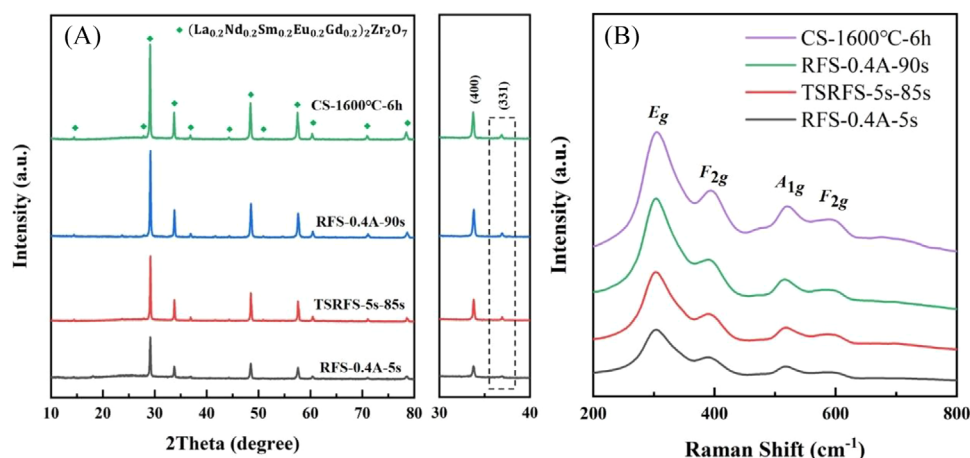

FIGURE 2 (A) X-ray diffraction (XRD) patterns (B) Raman spectra of flash sintered samples and pressurelessly sintered samples.

0.9 for a mixture of oxide ceramic. $\sigma = 5.67 \times 10^{-8}$ W m^{-2} K^{-4} is the Stefan-Boltzmann Constant.

XRD and Raman spectroscopy were used to characterize the phase of all samples. Figure 2 shows the XRD patterns and Raman spectrum of CS-1600°C-6 h, RFS-0.4 A-5s, RFS-0.4 A-90s, and TSRFS-5s-85s. It can be seen that all samples show only peaks of high-entropy $(La_{0.2}Nd_{0.2}Sm_{0.2}Eu_{0.2}Gd_{0.2})_2Zr_2O_7$, indicating that original oxides had been entirely reacted to high-entropy phase within 5 s after flash sintering occurred. Raman spectrum also demonstrated that all samples were in pyrochlore phase. This is in agreement with our previous work.[11]

Tests showed that the relative density of samples increased sharply from around 53% right before power spike (stage II) to around 77.6% right after power spike (RFS-0.4 A-0s). The calculated sample temperature of 1870°C at the power spike might at least partially explain the ultra-fast densification during power spike. As shown in Figure 3A, the relative density of RFS-0.4 A-5s (TSRFS-5s-0s) was around 89.6%, while the relative density of RFS-0.4 A-15s (TSRFS-15s-0s) and RFS-0.4 A-30s (TSRFS-30s-0s) was 94.3% and 96.5%, respectively. In other words, the relative density during step 1 of TSRFS samples increased slowly after 5s. Generally, with the same total duration, the relative density of TSRFS samples increased with longer duration in step 1. For example, the relative density of TSRFS-30s-60s was higher than TSRFS-15s-75s, and the relative density of TSRFS-15s-75s was higher than TSRFS-5s-85s. It is interesting that the relative densities of TSRFS-5s-25s, TSRFS-15s-15s and TSRFS-30 s-0s (also as RFS-0.4A-30s) were quite close to each other. One possible explanation is a "long tail effect" from the power spike. In conventional two-step sintering, samples are usually heated in the muffle or tube furnace to
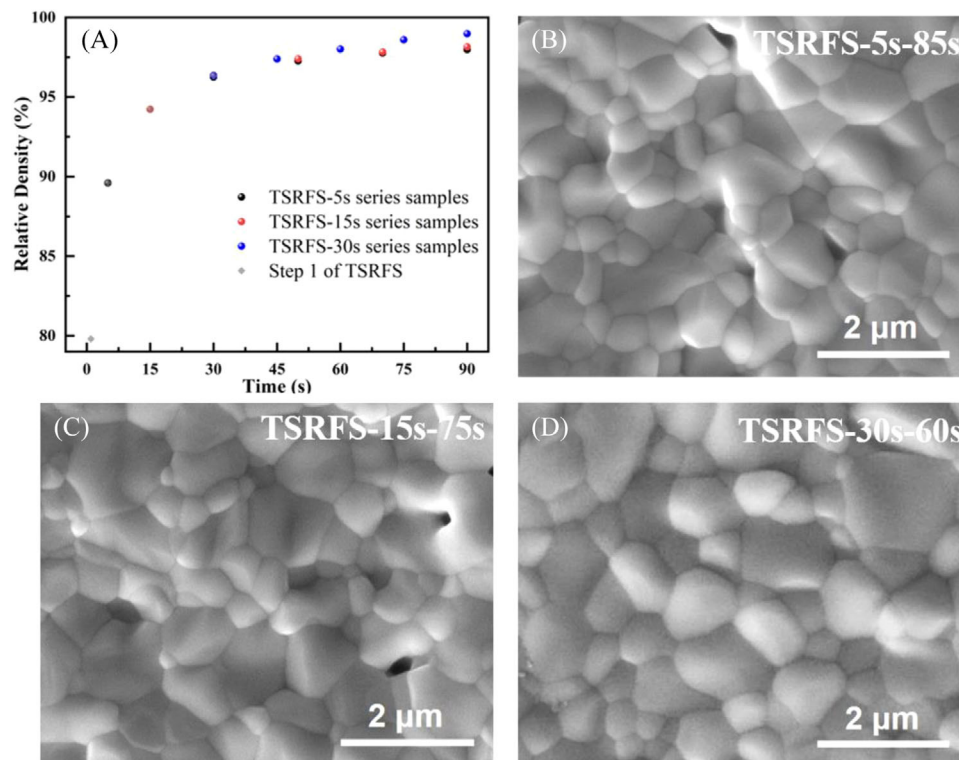
FIGURE 3 (A) Relative densities of two-step reactive flash sintering (TSRFS) samples with different holding time of step 2. Micrographs of flat surfaces of (B) TSRFS-5 s-85 s, (C) TSRFS-15 s-75 s, and (D) TSRFS-30 s-60 s.

a high temperature for a very short time and then cooled to a relatively lower temperature, and the heat flow is from the furnace to the sample surface via air. However, the volumetric heating caused by flash sintering makes sample temperatures much higher than the furnace temperature, so the real temperature at the core of the samples should be higher than the sample surface. Meanwhile, the thermal conductivity of $(La_{0.2}Nd_{0.2}Sm_{0.2}Eu_{0.2}Gd_{0.2})_2Zr_2O_7$ was reported as quite low, for example, only around 1 W m^{-1} K^{-1} at 1500°C.[16] Therefore, even a while after the power was switched to step 1 as in Figure 1, the real temperature inside the samples especially at the cores probably decreased slowly and remained still higher than 1595°C (corresponding to the current limit of 0.4 A in step 1 according to BBR). Such high temperature continued driving the densification for a while and was like a "long tail effect" from the power spike in step 0. This might explain why the power versus time schemes of TSRFS-5s-25s, TSRFS-15s-15s, and TSRFS-30s-0s were different (the total holding time were the same), but the overall relative densities of these three samples were quite close to each other. Figure 3B–D shows the representative microstructures of the flat surface of the TSRFS samples.

Grain sizes were measured from SEM pictures using a standard intercept method via software ImageJ (National Institutes of Health). Porosity at sample cores were also
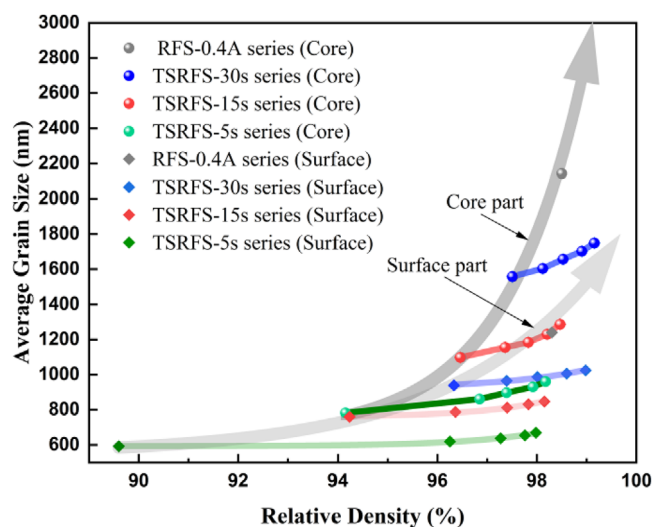

FIGURE 4 Grain size versus relative density at the surface and cores of samples prepared by reactive flash sintering (RFS) and two-step reactive flash sintering (TSRFS). For example, RFS-0.4A series (core) means the core part of RFS-0.4A series samples, while RFS-0.4A series (surface) means the surface part of RFS-0.4A series samples.

measured from SEM pictures and translated into relative density at cores. Figure 4 shows the plots of grain size versus relative density of both RFS and TSRFS specimens

TABLE 1 Wald-Wolfowitz tests representing if the grain size of the core and flat surface were considered equal with a 5% significance; the "×" symbolizes that the core and the surfaces had an equal average grain size, and then the sample was considered homogeneous, and "√" symbolizes the other way around.

Sample identification	Pass or not	Sample identification	Pass or not
RFS-0.4A-5s	×	TSRFS-15s-75s	√
TSRFS-5s-25s	×	RFS-0.4A-30s	√
TSRFS-5s-45s	×	TSRFS-30s-15s	√
TSRFS-5s-65s	×	TSRFS-30s-30s	√
TSRFS-5s-85s	×	TSRFS-30s-45s	√
RFS-0.4A-15s	√	TSRFS-30s-60s	√
TSRFS-15s-15s	√	RFS-0.4A-60s	√
TSRFS-15s-35s	√	RFS-0.4A-180s	√
TSRFS-15s-55s	√		

Abbreviations: RFS, reactive flash sintering; TSRFS, two-step reactive flash sintering.

on the flat surface and at the sample cores. The general relative density of samples right after power spike (RFS-0.4 A-0s) was around 77.6%, while the average grain size on the surface was around 348 nm and at the cores was around 398 nm. Therefore, it can be seen from Figure 4 that rapid final-stage grain growth happened in RFS samples, especially when the general relative density was above 90%. In contrast, it can be demonstrated that the grain growth both on the sample surface and at the sample cores was suppressed in the TSRFS samples compared with RFS samples. For example, TSRFS-5 s-85 s has a general relative density of around 97.9% with an average grain size of 669 nm on the surface and 945 nm at the cores, while the average grain size was 1165 nm on the surface and 1997 nm at the cores with identical density from interpolation of RFS. In addition, it is clear that the shorter the time in step 1, the smaller grain size (both surface and core) with identical densities in TSRFS samples. This is in agreement with traditional two-step pressureless sintering.[17]

It can be further demonstrated that applying TSRFS could reduce the grain size heterogeneity between the sample surface and core compared with RFS. Since the grain size distribution of the flash sintered samples in this work were all non-normal (see examples in Figure S2), Wald-Wolfowitz tests were employed to test if the grain size of the core and flat surface were considered equal with a 5% significance (Table 1). It can be seen that RFS-5s shows grain size homogeneity between the sample surface and core, but both RFS-15s and RFS-30s show grain size heterogeneity between sample surfaces and cores. TSRFS-5 s series samples all present grain size homogeneity between sample surfaces and cores. However, TSRFS-15

s and TSRFS-30 s series samples still present grain size heterogeneity between sample surfaces and cores. This indicates that longer duration in step 1 resulted in larger microstructural heterogeneity. This could be explained by the thermal gradient formed in dog-bone samples, which was enhanced by the low thermal conductivity of the high entropy pyrochlore (around 1 W·m^{-1}·K^{-1} at 1500°C),[16] making the sample cores more difficult to dissipate the heat compared with the sample surface, which might lead to a grain size gradients between sample surfaces and cores.[13,18–20] Similar phenomenon has been previously reported in 3YSZ system.[13,18] Since the short duration (5 s) under the current limit of 0.4 A in step 1 did not result in significant grain size heterogeneity between the surface and core, the grain size gradient increased relatively slowly in step 2 under the current limit of 0.32 A. This might explain why Wald-Wolfowitz tests showed no significant differences in grain size between the surface and the core of TSRFS-5s series samples. Lavagnini et al.[13] emphasized that high current limit either in step 1 or 2 of TSFS would lead to microstructural heterogeneity. One finding in this work different from Lavagnini et al.'s conclusion[13] is that besides the current limit, the time scheme during TSRFS played an important role in microstructural heterogeneity. Although the current limit in step 1 was high, TSRFS samples could still exhibit homogeneous microstructure between cores and sample surfaces as long as the time during step 1 was short. In other words, both the current limits and time of TSRFS should be comprehensively manipulated to achieve fast densification of high entropy pyrochlore along with fine grains and microstructural homogeneity.

4 | CONCLUSIONS

In summary, a TSRFS method was employed to achieve fast densification with suppressed grain growth and improved microstructural homogeneity in high entropy pyrochlore (La$_{0.2}$Nd$_{0.2}$Sm$_{0.2}$Eu$_{0.2}$Gd$_{0.2}$)$_2$Zr$_2$O$_7$. The art of efficient use of TSRFS lies in the reasonable manipulation of the time and power in steps 1 and 2 so that a balance between densification, grain growth, and microstructural homogeneity can be achieved.

CONFLICT OF INTEREST STATEMENT

The authors declare that they have no known competing financial interests or personal relationships that could have appeared to influence the work reported in this paper.

ORCID

Chen Xu https://orcid.org/0000-0002-1359-4923

_Na Ni_ https://orcid.org/0000-0002-2835-1326

REFERENCES

1. Weber WJ, Navrotsky A, Stefanovsky S, Vance ER, Vernaz E. Materials science of high-level nuclear waste immobilization. MRS Bull. 2009, 34;46–53.
2. Weber WJ, Ewing RC, Catlow CRA, Diaz de la Rubia T, Hobbs LW, Kinoshita C, et al. Radiation effects in crystalline ceramics for the immobilization of high-level nuclear waste and plutonium. J Mater Res. 1998, 13:1434–84.
3. Weber WJ, Ewing RC. Plutonium immobilization and radiation effects. Science. 2000, 289:2051–52.
4. Ewing RC, Weber WJ, Lian J. Nuclear waste disposal-pyrochlore ($A_2B_2O_7$): nuclear waste form for the immobilization of plutonium and "minor" actinides. J Appl Phys. 2004, 95:5949–71.
5. Zhou L, Li F, Liu J, Sun S, Liang Y, Zhang G. High-entropy $A_2B_2O_7$-type oxide ceramics: a potential immobilising matrix for high-level radioactive waste. J Haz Mater. 2021, 415:125596.
6. Xu L, Niu M, Wang H, Su L, Gao H, Zhuang L. Response of structure and mechanical properties of high entropy pyrochlore to heavy ion irradiation. J Eur Ceram Soc. 2022, 42:6624–32.
7. Teng Z, Zhu L, Tan Y, Zeng S, Xia Y, Wang Y, et al. Synthesis and structures of high-entropy pyrochlore oxides. J Eur Ceram Soc. 2020, 40:1639–43.
8. Biesuz M, Sglavo VM. Flash sintering of ceramics. J Eur Ceram Soc. 2019, 39:115–43.
9. Yoon B, Avila V, Lavagnini IR, Campos JV, Jesus LM. Reactive flash sintering of ceramics: a review. Adv Eng Mater. 2023, 25:2200731.
10. Yu M, Grasso S, Mckinnon R, Saunders T, Reece MJ. Review of flash sintering: materials, mechanisms and modelling. Adv Appl Ceram. 2017, 116:24-60.
11. Zhao G, Cai S, Zhang Y, Gu H, Xu C. Reactive flash sintering of high-entropy oxide $(La_{0.2}Nd_{0.2}Sm0_{.2}Eu_{0.2}Gd_{0.2})_2Zr_2O_7$: microstructural evolution and aqueous durability. J Eur Ceram Soc. 2023, 43:2593–600.
12. Nie J, Zhang Y, Chan JM, Jiang S, Huang R, Luo J. Two-step flash sintering of ZnO: fast densification with suppressed grain growth. Scr Mater. 2017, 141:6-9.
13. Lavagnini IR, Campos JV, Pallone EMJA. Microstructure evaluation of 3YSZ sintered by two-step flash sintering. Ceram Int. 2021, 47:21618–24.
14. Raj R. Joule heating during flash-sintering. J Eur Ceram Soc. 2012, 32:2293-301.
15. Todd RI, Zapata-Solvas E, Bonilla RS, Sneddon T, Wilshaw PR. Electrical characteristics of flash sintering: thermal runaway of Joule heating. J Eur Ceram Soc. 2015, 35:1865-77.
16. Li F, Zhou L, Liu J, Liang Y, Zhang G. High-entropy pyrochlores with low thermal conductivity for thermal barrier coating materials. J Adv Ceram. 2019, 8:576–82.
17. Chen IW, Wang XH. Sintering dense nanocrystalline ceramics without final-stage grain growth. Nature. 2000, 404:168–71.
18. Campos JV, Lavagnini IR, Pereira da Silva JG, Ferreira JA, Sousa RV, Mücke R, et al. Flash sintering scaling-up challenges: influence of the sample size on the microstructure and onset temperature of the flash event. Scr Mater. 2020, 186:1–5.
19. Pereira da Silva JG, Lebrun JM, Al-Qureshi HA, Janssen R, Raj R, Olevsky E. Temperature distributions during flash sintering of 8% yttria-stabilized zirconia. J Am Chem Soc. 2015, 98:3525–28.
20. Grasso S, Sakka Y, Rendtorff N, Hu C, Maizza G, Borodianska H, et al. Modeling of the temperature distribution of flash sintered zirconia. J Ceram Soc Japan. 2011, 119:3.

SUPPORTING INFORMATION

Additional supporting information can be found online in the Supporting Information section at the end of this article.